


Article

A Moving Bed Reactor for Thermochemical Energy Storage Based on Metal Oxides

Nicole Carina Preisner ^{1,*}  and Marc Linder ²¹ Institute of Engineering Thermodynamics, DLR, Linder Höhe, 51147 Köln, Germany² Institute of Engineering Thermodynamics, DLR, Pfaffenwaldring 38–40, 70569 Stuttgart, Germany; marc.linder@dlr.de

* Correspondence: nicole.preisner@dlr.de

Received: 4 February 2020; Accepted: 1 March 2020; Published: 6 March 2020



Abstract: High-temperature thermal energy storage enables concentrated solar power plants to provide base load. Thermochemical energy storage is based on reversible gas–solid reactions and brings along the advantage of potential loss-free energy storage in the form of separated reaction products and possible high energy densities. The redox reaction of metal oxides is able to store thermal energy at elevated temperatures with air providing the gaseous reaction partner. However, due to the high temperature level, it is crucial to extract both the inherent sensible and thermochemical energies of the metal-oxide particles for enhanced system efficiency. So far, experimental research in the field of thermochemical energy storage focused mainly on solar receivers for continuously charging metal oxides. A continuously operated system of energy storage and solar tower decouples the storage capacity from generated power with metal-oxide particles applied as heat transfer medium and energy storage material. Hence, a heat exchanger based on a countercurrent moving bed concept was developed in a kW-scale. The reactor addresses the combined utilization of the reaction enthalpy of the oxidation and the extraction of thermal energy of a manganese–iron-oxide particle flow. A stationary temperature profile of the bulk was achieved with two distinct temperature sections. The oxidation induced a nearly isothermal section with an overall stable off-gas temperature. The oxidation and heat extraction from the manganese–iron oxide resulted in a total energy density of 569 kJ/kg with a thermochemical share of 21.1%.

Keywords: moving bed; thermochemical energy storage; metal oxide

1. Introduction

A thermochemical energy storage (TCS) is able to complement concentrated solar thermal power plants (CSP) to allow for renewable base load supply. The principle of thermochemical energy storage is based on a chemically reversible gas–solid reaction. The thermal energy is either released in the form of reaction enthalpy (discharging), absorbed by the reverse endothermic reaction (charging), or stored in the chemical bond by the separation of the gas and solid phases. Thermochemical energy storage features high energy densities in comparison to other thermal energy storage concepts, i.e., sensible thermal energy storage or thermal energy storage based on a phase change [1,2]. Metal oxides are a suitable candidate for thermochemical energy storage for CSP, since the redox reaction of metal oxides occurs at elevated temperatures [3,4], which are necessary to reach high efficiencies. Furthermore, ambient air can provide the gaseous reaction partner, which simplifies gas handling in comparison to other TCS material systems. Therefore, the considered system (Figure 1) is based on metal-oxide particles as thermochemical energy storage material and heat transfer medium to expand the CSP operation time into evening hours or to compensate weather instability.

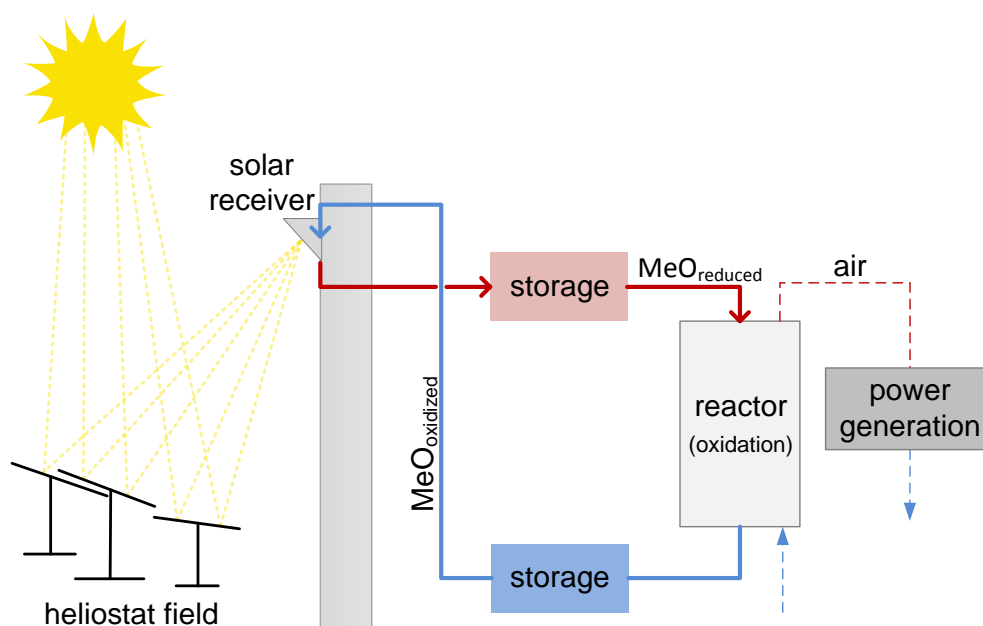


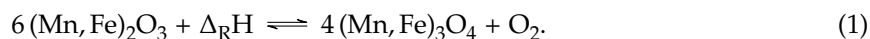
Figure 1. Concept of thermal energy storage based on metal-oxide particles for solar tower applications, including a high-temperature and low-temperature storage tank for decoupling of the system capacity and thermal power output.

The concept enables the decoupling of storage capacity and system power due to the continuously working heat exchanger and solar receiver and to the storage tanks in between. The metal-oxide particles are reduced by supplying concentrated solar irradiation until temperatures exceed the reduction onset temperature of the applied metal oxide. After an intermediate high-temperature storage tank, the discharging is performed in a separate reactor, optimized for oxidation. The particle loop is closed when the material is transported via an intermediate low-temperature storage tank back to the solar tower. Thus, a sufficient flowability of the metal-oxide particles is essential to implement the presented system concept. Schrader et al. [5] suggested a similar concept for thermochemical energy storage, where cobalt oxide is applied under pressurized conditions in a closed system. In addition, the utilization of particles as heat transfer and thermal storage material has been also investigated for sensible energy storage [6–8]. Owing to the high temperature level in the solar receiver, it is crucial to extract both the thermochemical energy and inherent sensible energy of the metal-oxide particles in the heat extraction reactor to enhance the total energy density and system efficiency.

The concept of combined extraction of sensible and thermochemical energy has been also suggested for inert honeycomb structures coated with a thermochemical energy storage material [9] and for the oxidation of CoO and subsequent cooling in pressurized air [5]. Furthermore, a solar-driven cycle based on copper oxide was proposed, where sensible, latent, and thermochemical energy of the metal oxide is extracted for high-temperature power generation and oxygen production [10]. In general and almost independent from the concept, the metal-oxide particles should meet several criteria for long-term utilization in the suggested continuous concept: sufficient mechanical strength, resistance of particle stability towards chemical and thermal stress, adequate chemical reversibility of redox reaction, high reaction enthalpy and heat capacity for enhanced energy density, affordable raw material cost, and low environmental impact due to the open system concept.

Recent work on metal oxides for the application as thermochemical energy storage includes binary metal oxides like $\text{Co}_3\text{O}_4/\text{CoO}$ [11] or perovskites like $\text{CaMnO}_{3-\delta}$ [12]. Furthermore, mixed metal oxides have been in focus lately, e.g., Mn–Fe oxides [13–16], Co–Mn oxides [17], and Co–Fe oxides [15,18]. The replacement of a primary oxide cation with a secondary cation can enhance the redox kinetics

and cycle stability in comparison to pure metal oxides [19]. For this work, manganese–iron oxide was chosen as a reference material to investigate the combined heat extraction of sensible and thermochemical energy. Phase diagrams of Mn–Fe oxides for ambient air condition predict a phase change between bixbyite $(\text{Mn, Fe})_2\text{O}_3$ and spinel phase $(\text{Mn, Fe})_3\text{O}_4$ for the considered Mn/(Mn + Fe) ratio of 0.7 via one or several two-phase regions [15,20–24]. Thus, the redox reaction follows the equation as below:



However, agglomeration of manganese–iron-oxide particles was reported, which could hinder the bulk movement in the considered continuous concept [25,26]. Consequently, we have investigated different supporting materials to improve the particle stability of manganese–iron oxide [26]. The addition of 20 wt.% ZrO_2 was found to enhance mechanical stability and to inhibit agglomeration. Manganese–iron-oxide particles are thus a promising candidate for a continuously operated system, and for this reason they were chosen for the system presented.

So far, solar receivers for metal-oxide reduction are mainly based on the rotary kiln concept [27–29] or applied as fluidized bed [30], packed bed reactor [31], and gravity-driven particle receivers [32–34]. The rotary-kiln concept already achieved wall temperatures up to 1000 °C in solar simulators [27,28]. A continuously operated particle receiver is favorable for CSP to allow for high mass flow rates, sufficient heat transfer between gas and solid phase, as well as decreased possible sintering effects [28]. Furthermore, a continuously working solar receiver needs to be heated up only once, which improves the thermal efficiency of the system. The oxidation of metal oxides for thermochemical storage application was investigated with packed bed reactors [19,25] and a fluidized bed reactor [35]. These reactors are suitable for the oxidation of metal oxides but do not allow for a continuous metal-oxide flow. However, this criterion is a basic requirement to realize the suggested system concept of Figure 1. Therefore, this work focuses on the heat extraction from metal-oxide particles in a continuously operated reactor.

In general, a circulating fluidized bed, flash reactor, moving bed reactor, or reactor with mechanical particle transport, e.g., rotary kiln or sintering band, is applicable for direct heat transfer from a continuous solid flow to a gas flow. In addition, the heat exchanger needs to ensure a particle residence time in the range of several minutes at temperatures suitable for oxidation according to a kinetic analysis of manganese–iron oxides with a similar cation ratio [14,16]. Furthermore, criteria like the ability to handle possible volume changes of the particles due to the reaction, heat transfer between gas and solid, possibility to extract thermochemical and sensible energy, and parasitic loss were taken into account.

The moving bed reactor concept has the advantage of low mechanical stress for the particles, low parasitic loss, no moving reactor parts, and a simple possibility to combine the utilization of sensible and thermochemical energy. The moving bed concept is also applied in an industrial scale, e.g., for a cooling cement clinker [36] or for the direct reduction of hematite to produce sponge iron [37,38]. In addition, the moving bed concept is used in chemical-looping combustion (CLC), where metal-oxide particles act as oxygen carriers to oxidize fuels in an oxygen-free atmosphere and reoxidize in air [39–41]. However, no continuously operated reactor for non-isothermal oxidation of metal oxides has been reported so far. Therefore, in this work, a moving bed reactor was designed for direct heat transfer between a metal-oxide particle flow in countercurrent to a gas flow for the discharging step of the system concept presented in Figure 1. Since an extraction of thermal energy leads naturally to a temperature decrease, the reaction rate of the thermochemical material is affected. Therefore, the influence of the reaction enthalpy release on the temperature profile of a stationary working moving bed reactor is investigated. Furthermore, the suitability of manganese–iron-oxide particles acting as a heat transfer material and thermal storage medium is explored.

2. Materials and Methods

2.1. Materials

The preparation of the manganese–iron-oxide particles was performed by VITO (Mol, Belgium) via build-up granulation, analogous to the procedure for metal-oxide particles in [16]. The raw materials Mn_3O_4 (Trimanox, Chemalloy), Fe_2O_3 (98% metal basis, Alfa Aesar), and ZrO_2 (99.9% ZrO_2 + HfO_2 , Saint Gobain) are mixed in powder form. A Mn/(Mn + Fe) ratio of 0.7 was chosen based on previous studies concerning cycle stability and reaction enthalpy [3,13,16]. The particles were heat treated for 10 h at 800 °C to obtain a bixbyite phase $(\text{Mn,Fe})_2\text{O}_3$ and sieved to a size between 2 mm and 3 mm. The obtained metal oxide is denoted $(\text{Mn}_{0.7}\text{Fe}_{0.3})_2\text{O}_3$ in the following. Based on our previous work, an addition of 20 wt.% ZrO_2 was chosen to improve particle stability and to inhibit agglomeration [26]. The material properties are summarized in Table 1.

Table 1. Material parameters of the manganese–iron-oxide particles.

Parameter	Symbol	Value/Correlation	Unit	Reference
Particle diameter	d_p	2–3	mm	as received
Bulk density	ρ_{bulk}	1400	kg/m ³	measured
Reaction enthalpy, based on oxidized phase	$\Delta_r H$	188	J/g	measured
Specific heat capacity of $(\text{Mn}_{0.7}\text{Fe}_{0.3})_2\text{O}_3$ + 20% ZrO_2 (30 °C to 580 °C)	c_{pox}	$427.76224 + 72.1084(\frac{T}{K} - 273.15)^{0.24307}$	J/kg/K	measured
True density of $(\text{Mn}_{0.7}\text{Fe}_{0.3})_2\text{O}_3$ + 20% ZrO_2	ρ_s	5204	kg/m ³	measured via He-pycnometry
Total porosity	ϵ	0.73	–	calculated
Bulk porosity	ϵ_b	0.48	–	calculated
Intra-particle porosity	ϵ_{por}	0.48	–	measured via Hg-intrusion-porosimetry

The bulk density of $1400 \text{ kg/m}^3 \pm 18 \text{ kg/m}^3$ was measured by filling and weighing a 250 mL cylinder. The effective onset temperature of reduction and oxidation was determined by means of thermogravimetric analysis (TGA) (STA 449 F3 Jupiter, Netzsch). Two metal-oxide particles with a total weight of around 30 mg were reduced and oxidized in an atmosphere of 20% oxygen (5.0) in nitrogen (5.0) by applying heating rates of 1, 5, 10, 20, or 30 K/min. The onset temperatures of each experiment were extrapolated with cubic spline method to null K/min for oxidation and reduction. The reaction enthalpy was examined with differential scanning calorimetry (DSC) for the oxidation applying heating rates of 10, 20, or 30 K/min at an oxygen partial pressure of 20 kPa. Based on the composite material in the oxidized phase, a reaction enthalpy of $188 \text{ J/g} \pm 8 \text{ J/g}$ was identified by taking the mean of the second to fourth cycle of each heating rate experiment. The value is in line with measurements in literature for $(\text{Mn}_x\text{Fe}_{1-x})_2\text{O}_3$ with a Mn/(Mn + Fe) ratio x of $x = 0.792$ (203 J/g [13]), $x = 0.75$ (271 J/g [16]), and $x = 0.67$ (162 J/g [3]). The specific heat capacity was measured in a temperature range of 30 °C to 580 °C by means of dynamic scanning calorimetry (DSC 204 F1 Phoenix, Netzsch). A heating and cooling rate of 10 K/min was applied with a nitrogen flow passing the pestled sample of $(\text{Mn}_{0.7}\text{Fe}_{0.3})_2\text{O}_3$ in a Pt/Rh crucible. Furthermore, a long time stability of the redox reaction was tested for 60 cycles in TGA. The mass loss indicated no decline during consecutive cycling (see Appendix A). More detailed properties related to particle stability of the applied manganese–iron-oxide compound can be found in Reference [26].

The reactor was never completely filled with metal-oxide particles. Sintered bauxite (type 30/50, Saint Gobain Proppants in USA) was selected as filling material for unheated reactor parts during

the reduction of the manganese–iron-oxide particles. The sintered bauxite particles have an average diameter of 0.47 mm and a bulk density of 2040 kg/m³. The effect of sintered bauxite on the reactivity of manganese–iron oxide was investigated during 30 redox cycles performed with TGA. For this analysis, the manganese–iron oxide was pestled and mixed with sintered bauxite particles. The sample was cycled in a Pt/Rh crucible without a lid between 850 °C and 1050 °C in a 100 mL/min gas stream with 20 vol % O₂ and nitrogen 5.0 as residual. The mass loss and gain due to the redox reaction stayed stable for all 30 cycles, and no side reactions were visible.

2.2. Experimental Setup

A reactor for direct heat exchange between a particle stream and air stream was designed based on a moving bed concept. The air stream flows in countercurrent to a moved particle bed, leading to a continuous heat transfer of inherent sensible and thermochemical energy. The gas stream provides O₂ for the reaction and would potentially act as heat transfer fluid to, e.g., a subsequent power generation cycle. The three functional sections of the reactor are displayed in Figure 2a.

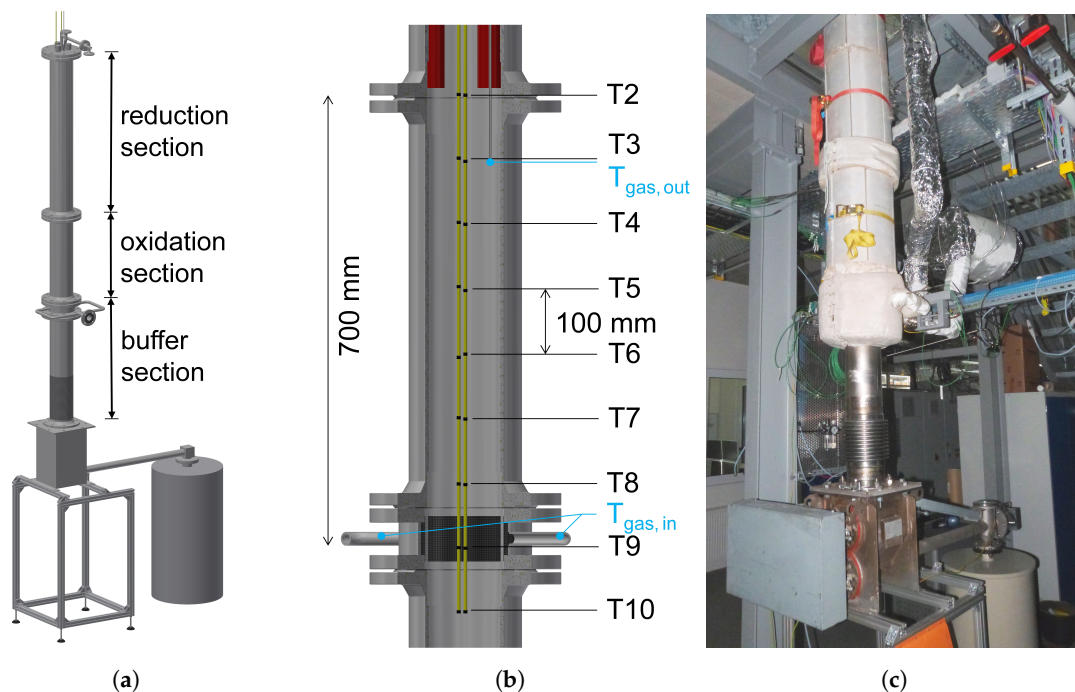


Figure 2. (a) Schematic of the reactor setup. (b) Close-up of the oxidation section with temperature measurement points. (c) Picture of assembled reactor.

Although the reactor is designed for the discharging of the metal-oxide particles, the upper reactor section, i.e., reduction section, corresponds to the solar receiver of the concept displayed in Figure 1. Three heating elements (Multicell, Watlow) inside the reactor tube (inner Ø: 152.3 mm) ensure a bed temperature above the reduction temperature of the applied metal-oxide particles. The heating elements are distributed centrosymmetrically to allow for homogeneous axial temperature distribution and are temperature regulated at three individual height sections to compensate the unequally distributed thermal losses in the reduction section. During the charging step, the whole metal-oxide bulk rests in the reduction section as a fixed bed on top of the filling material (sintered bauxite) in the residual reactor. The heat transfer between solid and gas is investigated in the oxidation section below the reduction section with moving bed conditions. High temperature-resistant wool and microporous silica isolation in height of the reduction and oxidation section reduces heat transfer to the environment. Two multipoint-thermocouples (type K, class 1, total Ø: 5 mm) are installed to measure the bulk temperature along the bed height at 9 levels every 100 mm in central and half

radial position in the oxidation section (see Figure 2b) and at a central height in the reduction section. The multipoint-thermocouples are composed of thermo wires embedded in MgO to reduce thermal conductivity between the measurement points and a 0.6 mm thin steel shell (nickel-based alloy 2.4816). The gas enters the reactor from two sides through a double-walled cylinder below the oxidation section. A filter (0.18 mm mesh size) prevents the particles from penetrating the gas tube system. The inlet gas temperature is analyzed with a thermocouple (\varnothing : 3 mm) in each gas inlet tube. The average temperature of both gas inlet flows is referred to as gas inlet temperature in later experiments. The gas is led through heated tubes or a separate gas heater for higher gas temperatures to preheat the gas to a set temperature at the inlet of the reactor. The off-gas temperature is analyzed by a thermocouple (\varnothing : 1 mm) enclosed in an open tube (\varnothing : 4 mm) at level T3 (see Figure 2b), which is connected to a pump of the gas analyzer. A small gas stream ($<20\text{ l/h}$) flows through the tube to the gas analyzer for oxygen measurement and improvement of heat transfer between gas flow and thermocouple. A screw conveyer regulates the particle volume flow at the bottom of the reactor to attain a moving bed condition. Agglomeration of manganese–iron-oxide particles after several consecutive cycles is reported [25,26] as well as fragmentation and breakage [26]. Thus, the metal–oxide particles are prevented from entering the dosing unit by a sieve (2.5 mm mesh size), which is located between the buffer section and the dosing unit as a precaution. The inert filling material can easily pass the sieve and is transported into a container connected to the screw conveyer. A knocking device is installed at the buffer section to support particle movement (Aldak, VTP-25, operated with 2 bar to 6 bar compressed air). In total, the reduction, oxidation, and buffer sections sum up to a height of 3.1 m.

The flow diagram of the setup is displayed in Figure 3. A mixture of compressed air (0 l/min to 200 l/min) and nitrogen 5.0 (0 l/min to 75 l/min) is regulated by two mass flow controllers (Bronkhorst HI-TEC, accuracy $\pm 0.5\%$ reading and $\pm 0.2\text{ l/min}$). All gas flow rates in this study are based on norm conditions ($T_{g,n} = 0^\circ\text{C}$ and $p_n = 1013.25\text{ hPa}$). The oxygen concentration in the off-gas is analyzed via paramagnetic oxygen measurement (NGA-2000 MLT-2, Emerson Process Management/Rosemount Analytical) and used to calculate the extent of conversion during the reduction and oxidation of the metal-oxide particles. The off-gas is cooled by a water-based cooling unit and filtered (high-efficiency particulate air filter) before entering the gas analyzer. Two pressure transducers ($-1/1\text{ bar}$ relative with an error $\pm 2\text{ mbar}$, B + B sensors) measure the pressure drop across the particle bed inside the reactor. The gas flow can bypass the reactor by adjusting the position of two throttle valves.

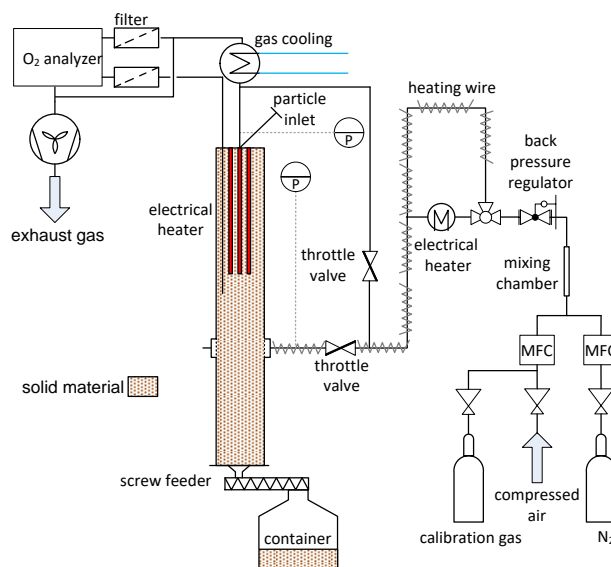


Figure 3. Flow diagram of the reactor setup.

2.3. Experimental Procedure

Prior to each metal-oxide experiment, the reactor was filled with bauxite and metal-oxide particles from the top. The buffer and oxidation section then consisted of bauxite particles, while the metal-oxide particles lay on top of the bauxite bulk in the reduction section. The experiment is composed of two segments: In the beginning, the metal-oxide bulk is reduced in a fixed bed operation (charging), followed by the oxidation under a moving bed condition (discharging). For the charging segment, the temperature of the heating elements was regulated to 1070 °C in order to reduce the metal-oxide particles in the reduction section. During this step, an air stream \dot{V}_n of 35 l/min flowed through the bulk at a gas inlet temperature $T_{g,in}$ of 480 °C to 500 °C. After 14.5 h of dwell time at a heating element temperature of 1070 °C, a bulk temperature of 1055 °C was measured at a central position in the reduction section. To foster the initial particle flowability for the subsequent moving bed operation, the heating element temperatures were reduced to 900 °C. Prior to this decrease of the bulk temperature, the gas flow was switched to a nitrogen flow for a period of 3 h to impede an early oxidation of the manganese–iron-oxide particles. The bulk movement for the moving bed experiment was induced and regulated by the screw conveyor by adjusting the volume flow rate. The dosing unit conveyed the bauxite particles in a connected container, while the metal-oxide bulk stayed in the buffer section, hindered by a filter, to minimize the mechanical stress for the metal-oxide particles. The gas flow was switched from nitrogen back to air before the metal-oxide bulk entered the oxidation section on top of the bauxite bulk. A reference moving bed experiment was performed with a metal-oxide particle flow of 3 g/s in countercurrent to an air flow \dot{V}_n of 150 l/min with a gas inlet temperature $T_{g,in}$ of 300 °C. The selected air flow should result in gas velocities below the minimal fluidization velocity of the manganese–iron-oxide bulk. After 4.5 h, the reduction and oxidation section was emptied of metal-oxide particles.

2.4. Conversion Calculation

The reaction conversion α of the redox reaction is calculated with the start mass of oxidized particles, oxygen concentration in the off-gas stream $c_{O_2,out}$, and the air flow $\dot{V}_{g,in}$ at the gas inlet, all of them being measured input parameters. A stoichiometric mass loss of 2.693% based on the oxidized phase results from the reaction equation (Equation (1)) for $(Mn_{0.7}Fe_{0.3})_2O_3 + 20 \text{ wt.}\% \text{ ZrO}_2$. A nitrogen balance yields the off-gas stream, with the assumption that the air entering the reactor only consists of O_2 and N_2 , N_2 being inert:

$$\dot{V}_{g,out} = \frac{\dot{V}_{g,in}(1 - c_{O_2,in})\rho_{N_2,in}}{(1 - c_{O_2,out})\rho_{N_2,out}}. \quad (2)$$

The oxygen concentration of the air flow $c_{O_2,in}$ at the gas inlet is fitted with the oxygen concentration in the off-gas $c_{O_2,out}$ when the reactor is under ambient condition, and thus, a nonreactive environment can be assumed. The difference of molar oxygen flow in and out of the reactor yields the molar amount of oxygen connected to the redox reaction. As a final step, the conversion α is calculated as a ratio of the accumulated molar uptake or release of oxygen due to the reaction $\dot{n}_{O_2,r}(t)$ to the stoichiometric molar oxygen release or uptake of the metal-oxide start mass $n_{O_2,s}$:

$$\alpha(t) = \frac{\sum_{t=0}^{t_{end}} \dot{n}_{O_2,r}(t) \times \Delta t}{n_{O_2,s}}. \quad (3)$$

3. Results and Discussion

The functional investigation of the installed moving bed reactor was performed with a manganese–iron-oxide particle flow in countercurrent to an air flow. Since the heat transfer of thermal and thermochemical energy can overlap in the moving bed reactor, the temperature and pressure dependence of the reaction rate of the redox reaction of the manganese–iron-oxide

particles is decisive. Therefore, in the first step, the reaction characteristics of the metal-oxide particles were examined regarding the effective onset temperatures as well as the pressure and temperature dependence on the reaction rate. In the next step, the effect of the release of reaction enthalpy on the temperature profile and reactor performance of a moving bed reactor was investigated experimentally. Finally, the suitability of the manganese-iron-oxide particles for application as heat transfer medium and thermochemical energy storage material in a moving bed reactor is discussed.

3.1. Reaction Characteristics

The effective onset temperature of the manganese-iron oxide is one crucial material parameter which influences the temperature profile of the moving bed reactor being studied. Dynamic thermogravimetric analyses yield a temperature threshold of 915.5 °C for the oxidation onset and 1003.1 °C for the reduction onset of the manganese-iron-oxide particles based on an oxygen partial pressure of 200 hPa (see Appendix B). This temperature difference is referred to as “thermal hysteresis” and was also reported for manganese-iron oxides with different cation ratios [14,16]. Apparently, reaction kinetics limit the conversion between 915.5 °C and 1003.1 °C in such an amount that this temperature area is technically irrelevant for a moving bed reactor. Nevertheless, the samples were reduced and oxidized to a conversion extent of at least 99% during all cycles of the applied heating and cooling rates between 1 K/min and 30 K/min. Therefore, two conclusions concerning the envisaged moving bed experiments can be drawn: Firstly, the oxidation of the manganese-iron-oxide particles will occur below the effective onset temperature of 915.5 °C, and finally, reaction kinetics should not limit the conversion for cooling rates up to 30 K/min in case of an oxygen partial pressure of 200 hPa.

As a next step, the temperature dependence on the reaction rate is analyzed with TGA. The obtained conversion during isothermal measurements between 500 °C and 925 °C is presented in Figure 4. The samples were reduced in a gas flow containing 21% oxygen at 1050 °C prior to the analysis of the oxidation reaction for a selected temperature. As a next step, to initiate the oxidation, the material was at first cooled to the specific temperature in nitrogen, and then after 5 min dwell time, it was exposed to a gas flow containing 21% oxygen. The reaction rate reaches its maximum between a temperature of 700 °C to 800 °C for the considered oxygen partial pressure of 210 hPa. Outside of this temperature range, the induction period is prolonged and the reaction rate decreases. Especially a solid temperature above 900 °C or below 550 °C drastically reduces the reaction rate. A minimal induction period of 1 min can be identified for all isothermal measurements in Figure 4b. Furthermore, the isothermal measurement at 925 °C indicates that the oxidation can be triggered above the previously determined onset temperature, although with a low reaction rate. Regarding the application in a moving bed, the operational conditions should allow for a particle residence time of at least 4 min in the temperature range of 700 °C to 800 °C to favor a full conversion of the material.

However, in contrast to the conditions in thermogravimetric analysis, the oxygen partial pressure will be reduced by oxidation in the moving bed experiment due to a higher ratio of particle mass to gas flow. Therefore, the pressure dependence of the reaction is examined using isothermal measurements at 850 °C (see Figure 5).

The measurements indicate a clear correlation between the oxygen partial pressure and the reaction rate. A lower oxygen partial pressure causes a lower reaction rate and prolongs the induction period of the reaction. Higher gas flows could therefore lead to an increased reaction conversion as they counteract the drop in oxygen partial pressure and thus increase the reaction rate.

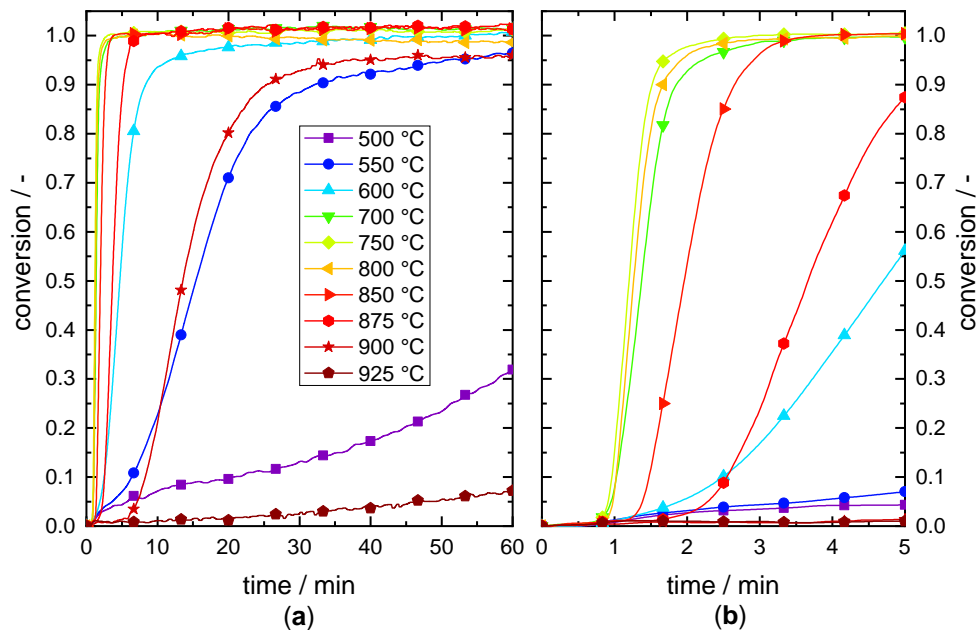


Figure 4. Oxidation conversion of manganese–iron oxide particles during isothermal measurements with an oxygen partial pressure of 210 hPa in a thermogravimetric analyzer. (a) Overview of the reaction conversion of the isothermal section. (b) Enlarged plot of the reaction conversion during the first 5 min of the isothermal section.

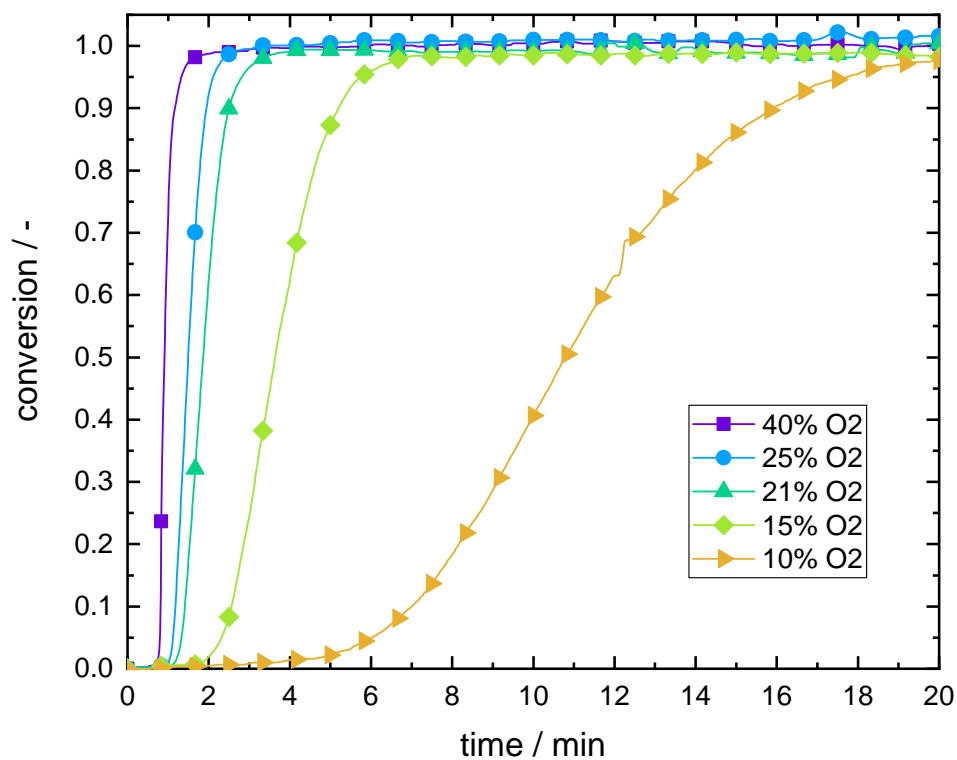


Figure 5. Isothermal oxidation of manganese–iron oxide particles with varying oxygen partial pressure in a thermogravimetric analyzer at 850 °C.

3.2. Experimental Results of a Moving Bed Reactor Operated with Mn–Fe-Oxide Particles

The interaction of the release of reaction enthalpy and the direct heat transfer of sensible thermal energy to a gas stream was investigated with a moving bed reactor based on metal-oxide particles. In Figure 6, the gas and solid temperatures during moving bed condition with a metal-oxide flow of 3 g/s in countercurrent to an air flow \dot{V}_n of 150 l/min are displayed together with the oxygen concentration in the off-gas. The diagram represents a period of the moving bed operation, when preheated manganese–iron-oxide particles continuously enter the oxidation section (compare Figure 2a). The position of the thermocouples in the oxidation section is given in the schematic next to the diagram.

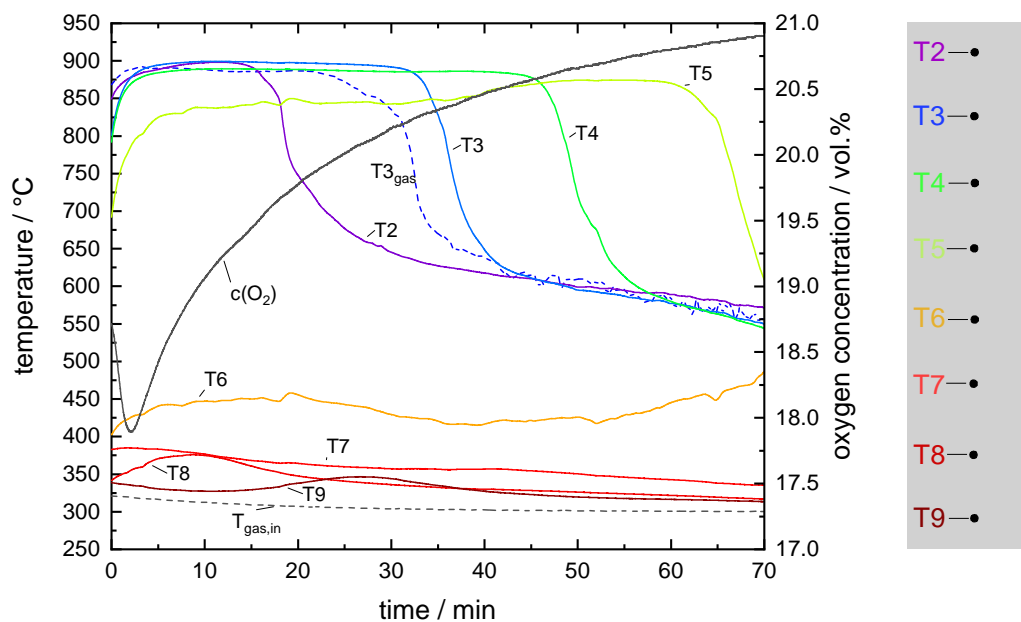


Figure 6. Solid (continuous line) and gas temperatures (dashed line) during moving bed operation with 3 g/s particle flow in countercurrent to an air flow \dot{V}_n of 150 l/min. The oxygen concentration in the exhaust gas is shown on the right axis of ordinate. The schematic of the oxidation section next to the diagram displays the temperature measurement points.

The bulk temperatures show a different course at different bed heights. In the first 20 cm of bed height (T2 to T4), the bulk temperature forms plateaus between 886 °C and 897 °C. The bulk temperature at level T5 increases with time to the temperature range of the temperature plateaus as well. The temperature drop at the end of each plateau marks the point in time when the top layer of the manganese–iron-oxide bulk falls below this measuring point. In contrast to the temperature plateaus between bed height level T2 to T5, the bulk temperature strongly decreases in the following 10 cm to bed height level T6. As a result, the bulk is cooled with a rate of 24 K/min in between those measurement points, considering the temperature change of the topmost layer of the metal-oxide bulk. The gas temperature at level T3 follows the course of the bulk temperature at the same bed height. Due to the heat transfer between the particle bed and the gas flow, the gas temperature increases from $T_{gas,in}$ to $T_{3,gas}$ by a maximum value of 580 K. This temperature increase correlates with the obtained thermal power of the reactor, which will be discussed in Section 3.3. The oxygen concentration strongly declines during the first 10 min, which can be attributed to the oxygen uptake caused by the oxidation reaction. However, the starting oxygen concentration in the off-gas is still on a low level because of the nitrogen atmosphere prior to the displayed period of the moving bed operation. In total, 80.2% of the former reduced particles were oxidized during moving bed operation. The initial heating period under fixed-bed condition resulted in an absolute reduction conversion of 77.1%. It has to be noted that the measured oxygen concentration provides the reaction condition as an average over the whole

bed. Therefore, the effect of oxidation on the oxygen concentration at a lower bed height could exceed the effect of reduction from the bulk close to the heating section of the reactor. This fact could result in a higher absolute conversion than calculated.

In Figure 7, the development of a temperature profile of several particle layers during the moving bed operation of the reactor with a Mn–Fe-oxide mass flow of 3 g/s is displayed. The temperature profile depicts the change in temperature when particle layers, in distance of 2 cm to each other, move through the oxidation section. The temperature of the first particle layer in Figure 7 at a bed height of 70 cm corresponds to the solid particle temperature which is measured after 3 min in Figure 6 at the level of T2. The temperature development of the particle layers is selected according to the theoretical bulk movement of 0.65 cm/min.

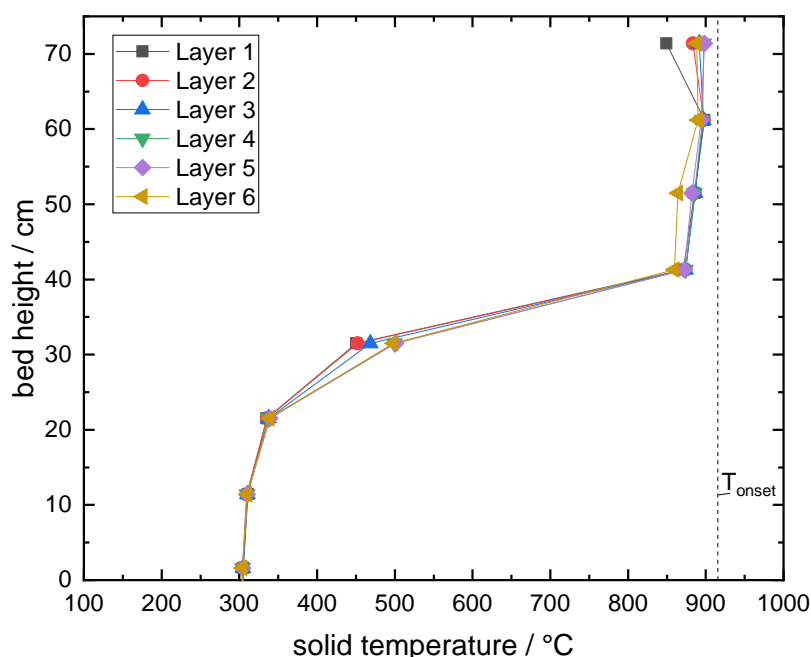


Figure 7. Development of the solid temperature of several layers (in 2 cm distance to each other) along the bed height in the oxidation section. The temperature development is selected according to the theoretical bulk movement. The effective onset temperature of the oxidation of the manganese–iron oxides is added as a dashed line.

The effect of the exothermic reaction is clearly visible by the nearly isothermal bed height of 30 cm. In general, the layers show a stationary temperature profile for the presented time period. Apparently, the amount of the released reaction enthalpy of the oxidation is able to compensate to a great extent for the heat transfer to the gas flow and thermal energy losses to the surrounding, e.g., thermal mass of reactor tube and heat transfer through insulation in the upper part (at bed height 40 cm to 70 cm) of this reactor setup. Overall, the solid temperature drops from 900 °C to 300 °C along the bed height. However, the particles reach the gas inlet temperature within a sharp front of ~20 cm. The lower part of the oxidation section (at bed height 0 cm to 20 cm) is again almost isothermal, however, in this case without chemical reaction. Thus, the reactor length could be shortened by around 20 cm without reducing the attained energy density of the thermochemical storage material or the thermal power of the moving bed reactor. The reproducibility of the formation of this characteristic nearly isothermal bed height is confirmed in Appendix C.

So far, it is unknown if the heat transfer of thermochemical and thermal energy overlap in the height section of high cooling rates. Obviously, oxidation takes part in the isothermal bed height. However, the experimental data does not describe the local oxygen concentration and thus conversion status. The determined reaction characteristics at different temperatures, cooling rates, or oxygen

partial pressures of the previous Section 3.1 can be applied to estimate the possibility of further reaction conversion in the section with a temperature gradient of the bulk. The moving bed experiment resulted in an oxidation conversion of 80.2% and temperature plateaus between 886 °C and 897 °C, which is below the effective onset temperature for oxidation of 915.5 °C. In TGA, the reaction requires 50 min at a sample temperature of 900 °C to attain a conversion extent of 96%, whereas full conversion is achieved after 5 min at 850 °C in case of 20% oxygen in the atmosphere (see Figure 4). The residence time of the particles in the nearly isothermal bed height of the moving bed reactor is around 50 min, considering a particle velocity of 0.65 cm/min. Thus, if the effect of the oxygen partial pressure can be neglected, the particles should be oxidized in the bed height of nearly isothermal conditions before their temperature is decreased to 300 °C. Furthermore, the attained cooling rates in the moving bed experiment depicted in Figure 6 are in the range of the investigated cooling rates of TGA measurements (Figure A2), where the extent of oxidation conversion was determined to exceed 99% for cooling rates of up to 30 K/min. However, as a minimal oxygen concentration of 17.9% was measured during the moving bed experiment, the oxygen partial pressure in the moving bed experiment was lower than the applied oxygen partial pressure in the TGA measurements regarding the temperature dependence of the reaction rate or the determination of onset temperatures for various cooling rates. Isothermal measurements at 850 °C based on TGA indicated that a decrease of oxygen concentration from 21% to 15% doubles the reaction time required to achieve an oxidation conversion of 99% (see Figure 5). In the end, the metal-oxide particles probably continued oxidizing in the section with high temperature gradients below the bed height with nearly isothermal conditions, which would result in overlapping heat transfer of thermochemical and thermal energy. An additional simulation of the presented moving bed experiment could yield the local extent of conversion caused by this complex correlation between chemical reaction and heat transfer.

3.3. Energetic Evaluation of the Moving Bed Reactor

The heat transfer between gas and solid is the main task of the presented moving bed reactor. Even though the gas temperature is difficult to measure at these elevated temperatures, the thermal power of the heat exchanger is estimated with $P_{th} = \int \dot{V}_{g,in} \rho_{g,norm} c_{p_g}(T) dT_g$. Here, $c_{p_g}(T)$ equals the temperature dependent specific heat capacity of the gas flow $\dot{V}_{g,in}$, which is stated for the gas density at norm condition $\rho_{g,norm}$. Figure 8 displays the attained thermal power during the period of moving bed operation corresponding to Figure 6. The gas temperature at level T3 directly determines the course of the thermal power curve, since the gas inlet temperature is nearly constant. The thermal power is nearly constant when particles with a stationary inlet temperature entered the oxidation section and drops, as soon as the top of the bulk passed level T3. From this moment on, the available bulk height for heat exchange decreases with time. Overall, the experiment achieved a peak power of 2.1 kW and an average power of 2.0 kW for 30 min.

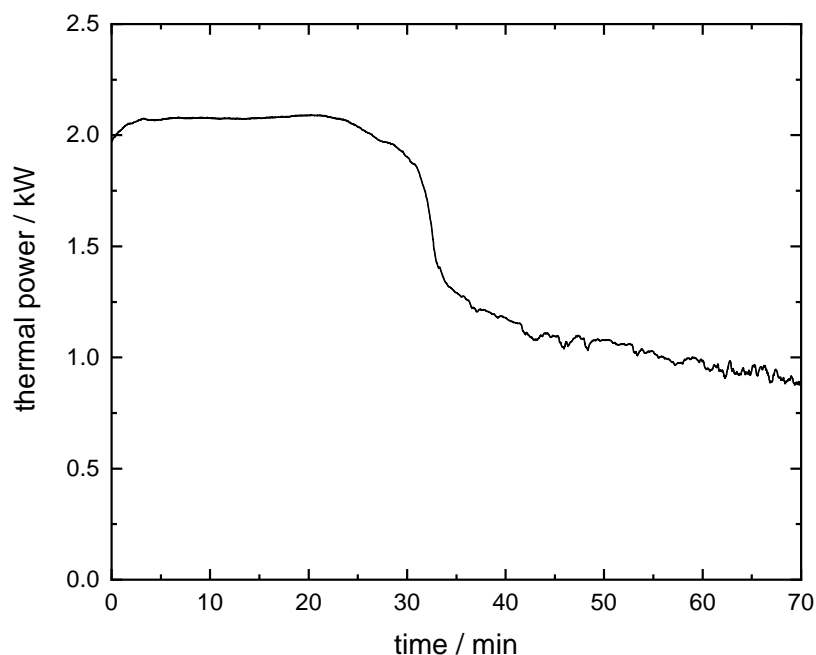


Figure 8. Attained thermal power of the moving bed reactor, which is transferred to the gas flow (150 l/min) by the countercurrent metal-oxide flow of 3 g/s: The displayed period of moving bed operation equals the period shown in Figure 6.

The energy density is a crucial factor to compare energy storage materials. Since the presented reactor facilitates the heat transfer of sensible as well as thermochemical energy to the countercurrent gas flow, the energy density of the manganese–iron-oxide particles is increased by the sensible share in energy density in comparison to other thermochemical energy storage materials. The manganese–iron-oxide particles entered the oxidation section of the reactor with 895 °C at position T3 and exited the oxidation section with 304 °C at T9. The gravimetric energy density of the metal-oxide particles can be calculated based on the specific heat capacity for the oxidized phase and the reaction enthalpy of 188 J/g (see Section 2). As a result, an energy density of 569 kJ/kg (or 158 Wh/kg) is achieved with the investigated metal-oxide particles and reactor setup, based on the oxidized phase of the material ($(\text{Mn}_{0.7}\text{Fe}_{0.3})_2\text{O}_3 + 20\text{wt.}\% \text{ ZrO}_2$). Here, the thermochemical share in energy density accounts for 21.1 %.

In conclusion, the concept of combined utilization of the release of reaction enthalpy and heat transfer of sensible thermal energy in a countercurrent moving bed reactor is feasible. The manganese–iron oxide was reoxidized to an extent of 80.2% relative to the extent of previous reduction. To improve the extent of oxidation conversion, three options are conceivable: Firstly, it is beneficial to increase the oxygen partial pressure during the moving bed operation to impede the limitations of the reaction kinetics. However, raising the oxygen partial pressure beyond ambient conditions would negate the advantage of simple gas handling when utilizing metal oxides as thermochemical energy storage. Secondly, lower solid flow rates would cause a higher particle residence time in a temperature range relevant for higher reaction rates, but it would also decrease the thermal power. Finally, an indirect heat transfer in the bed height of the nearly isothermal condition has the potential to lower the solid temperature to a level that allows for higher reaction rates without the need to decrease the total gas flow. For example, the gas flow could be first heated indirectly by the bed height of the nearly isothermal condition before entering the moving bed reactor for the heat transfer of sensible thermal energy. However, this would lead to higher solid outlet temperatures and thus a reduced utilization of the inherent thermal energy. In addition, the indirect heat transfer in the bed height of nearly isothermal conditions could power other high temperature processes, such as a thermoelectric generator or an alkali-metal thermal to electric converter.

3.4. Particle Handling in a Moving Bed Reactor Based on Manganese–Iron Oxide

The flowability of manganese–iron-oxide particles at elevated temperatures posed a major challenge when performing moving bed experiments. Especially the initiation of the metal-oxide movement after the particles were heated in the reduction section of the reactor (see Figure 2a) caused a discontinuous particle flow during most of the experiments, which are not presented in this study. In addition, the subsequent particle movement through the different sections of the reactor was aided by a knocking device and partial manual knocking on the buffer section. The blocking of the particles in the reactor tube after being heated and reduced in fixed bed operation emphasizes the necessity of a continuously working solar receiver. Concerning the presented metal-oxide experiment, the cooling of the manganese–iron-oxide particles in nitrogen atmosphere to around 905 °C particle temperature in combination with several pressure surges resulted in a successful initiation of the moving bed operation.

Agglomeration of the particles could constitute one reason for the low flowability of the metal-oxide bulk. However, our previous work about the particle stability of the same manganese–iron oxide did not indicate a high tendency towards agglomeration [26]. A picture of the uppermost layer of the metal-oxide bulk after the moving bed experiment is displayed in Figure 9b. For this purpose, the reactor was opened between the oxidation section and the buffer section. No agglomerates or channels were discovered after this experiment. Furthermore, Figure 9a depicts an exemplary amount of metal-oxide particles in the untreated condition (1) or after 15 experiments in the moving bed reactor (2). The comparison reveals no visible change in particle constitution.

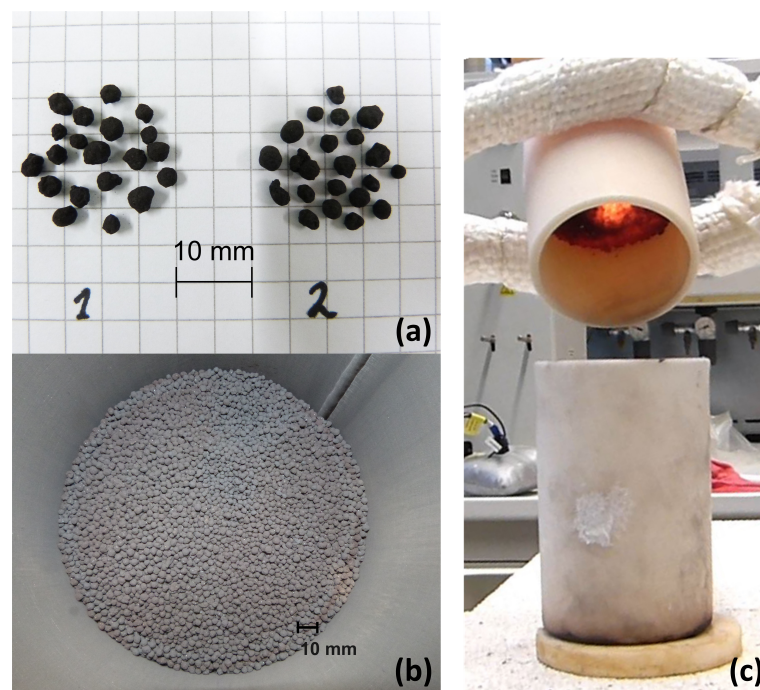


Figure 9. (a) Comparison of fresh manganese–iron oxide particles (1) to manganese–iron oxide particles after 15 redox cycles in the moving bed reactor (2). (b) Picture of the uppermost bulk layer after the described moving bed experiment. (c) Picture of the flowability tests performed after the sample was extracted from the chamber furnace set at 1050 °C.

The flowability of the metal-oxide bulk in the reactor setup was tested at room temperature with a particle flow of 3 g/s. The velocity of the uppermost particle layer was determined and compared with the theoretical velocity, which was obtained by calibrating the screw conveyor. The agreement of the experimental velocity with the theoretical velocity proves the basic flowability of the material at room temperature. Therefore, the temperature dependence of the particle flowability was additionally

investigated. An amount of 100 g manganese–iron oxide particles was filled in a ceramic beaker and cycled between temperatures of 50 °C and 1050 °C in a chamber furnace with ambient atmosphere. The metal-oxide sample was extracted from the furnace at different temperatures and transferred into an empty ceramic beaker to examine the flowability. The picture in Figure 9c illustrates a time section of the particle transfer when the sample was extracted from the furnace at 1050 °C with a measured sample temperature of 1034 °C initially to the decanting process. At this high temperature, the sample was initially stuck in the ceramic beaker. Over several stages, the sample then flowed into the empty beaker within a cooling time of 2 min, requiring slight shaking movements or knocking of the beaker onto a refractory brick. The sample was transferred back to the original ceramic beaker without difficulty at a particle temperature of around 700 °C to 860 °C. Repeating the decanting process between 850 °C and 1050 °C confirmed the reduced flowability, whereas the particles were free flowing at a sample temperature of 550 °C. In summary, the flowability of the manganese–iron oxide particles is limited, when they are previously heated as a fixed bed to temperatures between 850 °C and 1050 °C.

4. Conclusions

The first moving bed reactor for thermochemical energy storage at high temperatures has been put into operation and analyzed in detail. The reactor addressed the combined utilization of thermochemical and sensible energy based on metal-oxide particles, which is important to enhance the system efficiency. The reaction behavior of the material at different temperatures and pressures was investigated to pretest the reaction capability at probable experimental operation conditions. Furthermore, the suitability of the manganese–iron oxide was assessed for application in a continuously operated system. The main conclusions considering technical applications are as follows:

- Thermogravimetric analyses revealed that cooling rates of up to 30 K/min pose no challenge for the oxidation of the investigated manganese–iron oxide at an oxygen partial pressure of 20 kPa. Furthermore, sufficient long-term stability of the redox reaction was demonstrated for 60 consecutive cycles in TGA.
- The oxidation of the manganese–iron oxide caused two distinct temperature sections during the moving bed experiment: one section with nearly isothermal conditions and one section with a temperature gradient similar to a moving bed operation based on inert storage material. A thermal power of 2 kW was transferred to the gas flow during stationary temperature conditions.
- The manganese–iron oxide particles were oxidized to an extent of 80.2% during moving bed operation, based on the preceding partial reduction of 77.1%. An indirect heat transfer in the section of nearly isothermal condition could increase the oxidation conversion because the particle temperature could be regulated to a level of higher reaction rates.
- The flowability of the manganese–iron-oxide particles was limited at high temperatures in the moving bed reactor. Additional tests revealed an insufficient flowability between 850 °C and 1050 °C. However, the underlying mechanism needs to be further addressed for an application of this manganese–iron oxide compound in a continuously operated system.

Author Contributions: Conceptualization, N.C.P. and M.L.; methodology, N.C.P. and M.L.; software, N.C.P.; validation, N.C.P. and M.L.; formal analysis, N.C.P.; investigation, N.C.P.; resources, N.C.P.; data curation, N.C.P.; writing—original draft preparation, N.C.P.; writing—review and editing, M.L.; visualization, N.C.P.; supervision, M.L.; project administration, M.L.; funding acquisition, M.L. All authors have read and agreed to the published version of the manuscript.

Funding: This research received no external funding.

Acknowledgments: The authors wish to thank Andreas Kohzer, Niklas Giesen (both Institute of Thermodynamic Engineering, German Aerospace Center, Cologne, Germany), and Sofie Ek (Department of Chemistry and Chemical Engineering, Chalmers University of Technology, Gothenburg, Sweden) for their support while assembling the reactor and running experiments. Furthermore, the authors thank Andrea Hanke (Institute of Thermodynamic Engineering, German Aerospace Center, Stuttgart, Germany) for performing the DSC to

examine the specific heat capacity of the metal-oxide particles and Henrik Winnemöller (Johannes Gutenberg University Mainz, Mainz) for proofreading.

Conflicts of Interest: The authors declare no conflict of interest.

Appendix A. Cycle Stability of the Redox Reaction of Mn–Fe Oxide

Two consecutive cycling tests, consisting each of 30 redox cycles, were carried out in TGA with a heating and cooling rate of 20 K/min at an oxygen partial pressure of 20 kPa. The first 30 cycles were performed between a sample temperature of 850 °C and 1050 °C, whereas the lower sample temperature was decreased to 750 °C for the following 30 cycles. Figure A1 depicts the mass loss of exemplary cycles. Both the reduction and oxidation indicate a stable mass loss over 60 redox cycles.

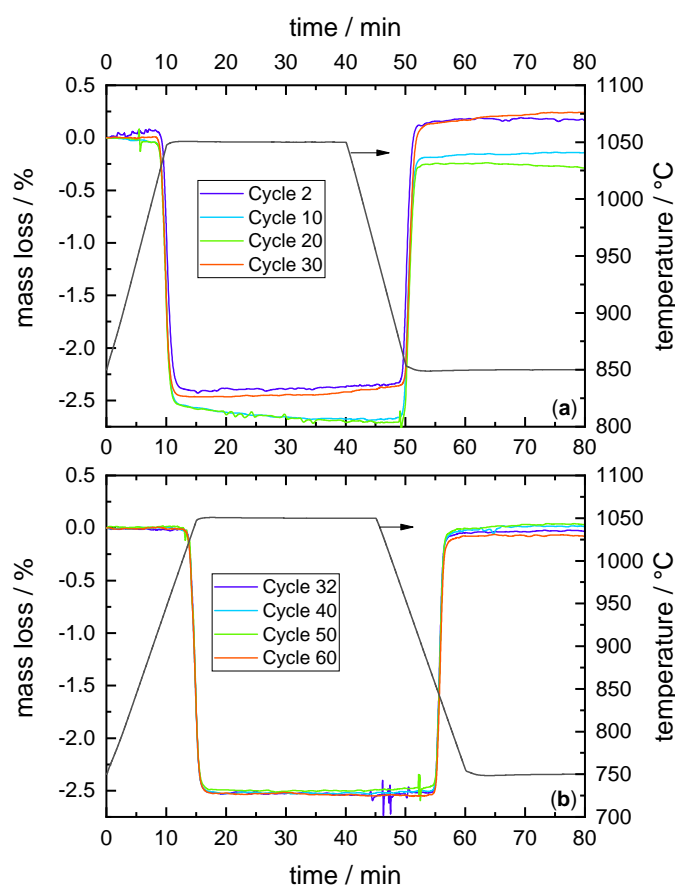


Figure A1. Relative mass loss of the manganese–iron oxide compound during several redox cycles performed in TGA with an oxygen partial pressure of 20 kPa and a heating and cooling rate of 20 K/min. (a) The sample temperature was varied between 850 °C and 1050 °C during the first 30 redox cycles. (b) The next 30 redox cycles were carried out between a sample temperature of 750 °C and 1050 °C.

Appendix B. Determination of the Effective Onset Temperature of the Investigated Mn–Fe Oxide

The effective onset temperature of the oxidation and reduction of the transition of $(\text{Mn}_{0.7}\text{Fe}_{0.3})_3\text{O}_4/(\text{Mn}_{0.7}\text{Fe}_{0.3})_2\text{O}_3$ is determined via thermogravimetric analysis. Dynamic measurements with 1–5–10–20 and 30 K/min heating or cooling rate and an atmosphere of 20% oxygen were performed. The extrapolation to 0 K/min of the average onset temperatures of 3 cycles with different heating or cooling rates yields the effective onset temperature and is displayed with dashed lines in Figure A2 for oxidation and reduction.

Obviously, the effective onset temperature of the reduction deviates from the effective onset temperature of the oxidation. A temperature difference of 87.6 °C between the two onset temperatures

is found for the applied oxygen partial pressure and is referred to as thermal hysteresis of the redox reaction. The gained temperature borders do not equal the thermodynamic equilibrium, which was calculated with Factsage (phase transition: bixbyite + spinel to bixbyite). However, the effective onset temperatures constitute a technical temperature threshold for the application of the Mn–Fe oxide under ambient atmospheric conditions.

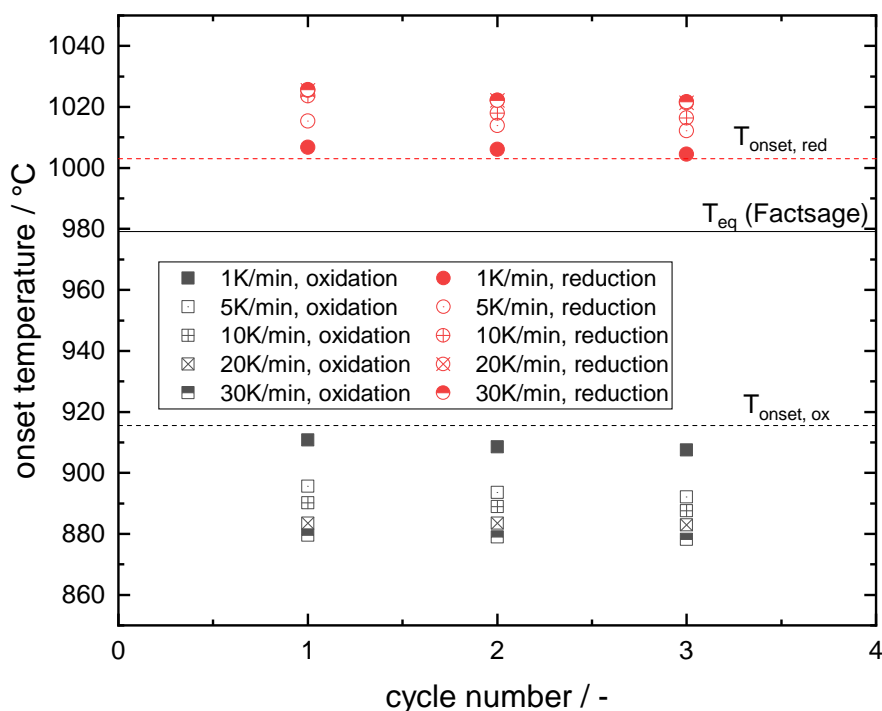


Figure A2. Obtained onset temperatures of reduction and oxidation of the investigated manganese–iron oxide for 3 consecutive cycles in a thermogravimetric analyzer, applying an oxygen concentration of 20% at different heating and cooling rates: The effective onset temperatures (dashed lines) and the thermodynamic equilibrium (solid line) are displayed as well.

Appendix C. Reproducibility of the Characteristic Isothermal Bed Segment

The development of the solid temperature of several particle layers during nearly steady-state operation of the moving bed experiment presented in this study is compared to an additional moving bed experiment in Figure A3. The additional experiment was performed with the same particle flow rate but a lower gas flow rate and gas inlet temperature. The characteristic isothermal bed segment (bed height of 40 cm to 70 cm), which is caused by the oxidation, is identical for both experiments in position and temperature. The following segment (bed height 10 cm to 40 cm), where the temperature profile is dominated by the sensible cooling of the particle layers, indicates a lower temperature gradient for the additional experiment. This variation between the temperature profiles could be caused by the lower gas flow and an insufficient particle flowability in the additional experiment. Due to the inconsistent particle movement, the results of the additional experiment are not discussed in more detail. Nevertheless, they corroborate the reproducibility of the characteristic temperature profile of a countercurrent moving bed based on a thermochemical material in principle.

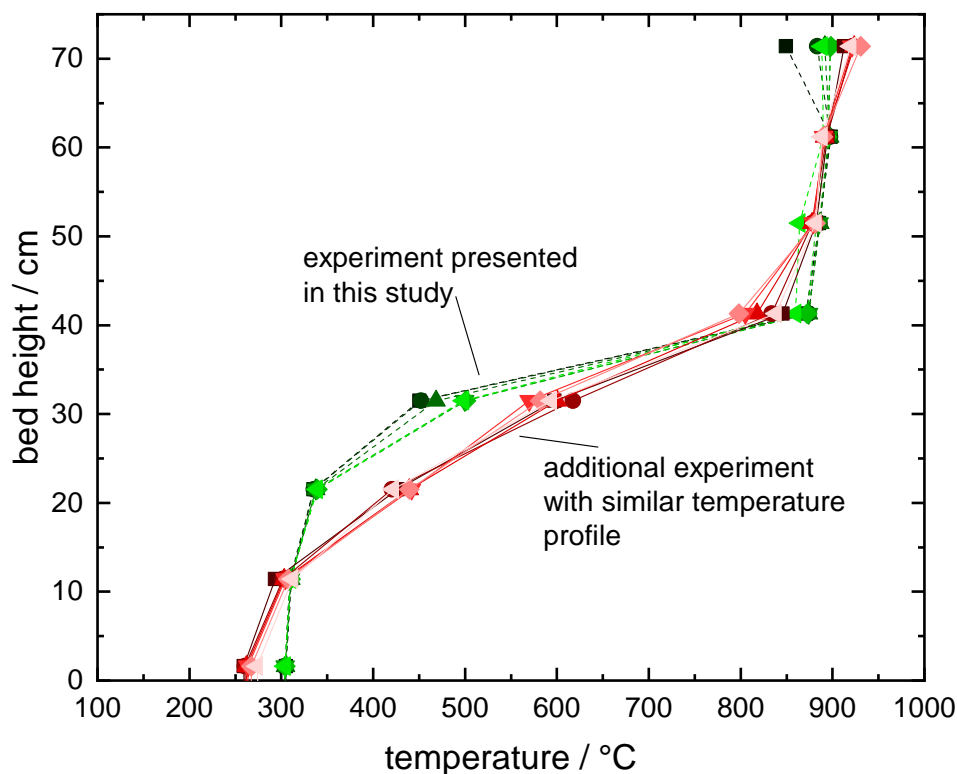


Figure A3. Development of the temperature of 6 particle layers (in 2 cm distance to each other) along the bed height during moving bed operation of the experiment in the study (green dotted lines, compare to Figure 7) and a similar experiment (red solid lines).

References

- Pardo, P.; Deydier, A.; Anxionnaz-Minvielle, Z.; Rougé, S.; Cabassud, M.; Cognet, P. A review on high temperature thermochemical heat energy storage. *Renew. Sustain. Energy Rev.* **2014**, *32*, 591–610, doi:10.1016/j.rser.2013.12.014.
- Wu, S.; Zhou, C.; Doroodchi, E.; Nellore, R.; Moghtaderi, B. A review on high-temperature thermochemical energy storage based on metal oxides redox cycle. *Energy Conv. Manag.* **2018**, *168*, 421–453, doi:10.1016/j.enconman.2018.05.017.
- Block, T.; Schmücker, M. Metal oxides for thermochemical energy storage: A comparison of several metal oxide systems. *Solar Energy* **2016**, *126*, 195–207, doi:10.1016/j.solener.2015.12.032.
- André, L.; Abanades, S.; Flamant, G. Screening of thermochemical systems based on solid-gas reversible reactions for high temperature solar thermal energy storage. *Renew. Sustain. Energy Rev.* **2016**, *64*, 703–715, doi:10.1016/j.rser.2016.06.043.
- Schrader, A.J.; Muroyama, A.P.; Loutzenhiser, P.G. Solar electricity via an Air Brayton cycle with an integrated two-step thermochemical cycle for heat storage based on $\text{Co}_3\text{O}_4/\text{CoO}$ redox reactions: Thermodynamic analysis. *Sol. Energy* **2015**, *118*, 485–495, doi:10.1016/j.solener.2015.05.045.
- Falcone, P.K.; Noring, J.E.; Hacket, C.E. Evaluation and application of solid thermal energy carriers in a high temperature solar central receiver system. In Proceedings of the IECEC 17th Intersociety Energy Conversion Engineering Conference, Los Angeles, CA, USA, 8–12 August 1982.
- Siegel, N.; Kolb, G. Design and on-sun testing of a solid particle receiver prototype. In Proceedings of the ASME 2008 2nd International Conference on Energy Sustainability, ASMEDC, Jacksonville, FL, USA, 10–14 August 2008; Volume 2, doi:10.1115/es2008-54090.
- Flamant, G.; Gauthier, D.; Benoit, H.; Sans, J.L.; Garcia, R.; Boissière, B.; Ansart, R.; Hemati, M. Dense suspension of solid particles as a new heat transfer fluid for concentrated solar thermal plants: On-sun proof of concept. *Chem. Eng. Sci.* **2013**, *102*, 567–576, doi:10.1016/j.ces.2013.08.051.

9. Agrafiotis, C.; de Oliveira, L.; Roeb, M.; Sattler, C. A solar receiver-storage modular cascade based on porous ceramic structures for hybrid sensible/thermochemical solar energy storage. In *SolarPACES, AIP Conference Proceedings*; AIP Publishing LLC: Melville, NY, USA, 2016; Volume 1734, doi:10.1063/1.4949099. ISBN 978-0-7354-1386-3.
10. Jafarian, M.; Arjomandi, M.; Nathan, G.J. Thermodynamic potential of molten copper oxide for high temperature solar energy storage and oxygen production. *Appl. Energy* **2017**, *201*, 69–83, doi:10.1016/j.apenergy.2017.05.049.
11. Agrafiotis, C.; Roeb, M.; Schmücker, M.; Sattler, C. Exploitation of thermochemical cycles based on solid oxide redox systems for thermochemical storage of solar heat. Part 1: Testing of cobalt oxide-based powders. *Sol. Energy* **2014**, *102*, 189–211, doi:10.1016/j.solener.2013.12.032.
12. Imponenti, L.; Albrecht, K.J.; Kharait, R.; Sanders, M.D.; Jackson, G.S. Redox cycles with doped calcium manganites for thermochemical energy storage to 1000 °C. *Appl. Energy* **2018**, *230*, 1–18, doi:10.1016/j.apenergy.2018.08.044.
13. Carrillo, A.J.; Serrano, D.P.; Pizarro, P.; Coronado, J.M. Improving the thermochemical energy storage performance of the Mn₂O₃/Mn₃O₄ redox couple by the incorporation of iron. *ChemSusChem* **2015**, *8*, 1947–1954, doi:10.1002/cssc.201500148.
14. Carrillo, A.J.; Serrano, D.P.; Pizarro, P.; Coronado, J.M. Understanding redox kinetics of iron-doped manganese oxides for high temperature thermochemical energy storage. *J. Phys. Chem. C* **2016**, *120*, 27800–27812, doi:10.1021/acs.jpcc.6b08708.
15. André, L.; Abanades, S.; Cassayre, L. High-temperature thermochemical energy storage based on redox reactions using Co-Fe and Mn-Fe mixed metal oxides. *J. Solid State Chem.* **2017**, *253*, 6–14, doi:10.1016/j.jssc.2017.05.015.
16. Wokon, M.; Block, T.; Nicolai, S.; Linder, M.; Schmücker, M. Thermodynamic and kinetic investigation of a technical grade manganese-iron binary oxide for thermochemical energy storage. *Solar Energy* **2017**, *153*, 471–485, doi:10.1016/j.solener.2017.05.045.
17. Carrillo, A.J.; Moya, J.; Bayón, A.; Jana, P.; de la Peña O’Shea, V.A.; Romero, M.; Gonzalez-Aguilar, J.; Serrano, D.P.; Pizarro, P.; Coronado, J.M. Thermochemical energy storage at high temperature via redox cycles of Mn and Co oxides: Pure oxides versus mixed ones. *Solar Energy Mat. Solar Cells* **2014**, *123*, 47–57, doi:10.1016/j.solmat.2013.12.018.
18. Block, T.; Knoblauch, N.; Schmücker, M. The cobalt-oxide/iron-oxide binary system for use as high temperature thermochemical energy storage material. *Thermochim. Acta* **2014**, *577*, 25–32, doi:10.1016/j.tca.2013.11.025.
19. Wong, B. *Thermochemical Heat Storage for Concentrated Solar Power*; Technical Report; Phase II Final Report for the period September 30, 2008 through April 30, 2011; U.S. Department of Energy: Washington, DC, USA, 2011.
20. Muan, A.; Somiya, S. The system iron oxide-manganese oxide in air. *Am. J. Sci.* **1962**, *260*, 230–240.
21. Wickham, D.G. The chemical composition of spinels in the system Fe₃O₄-Mn₃O₄. *J. Inorg. Nucl. Chem.* **1969**, *31*, 313 – 320.
22. Crum, J.V.; Riley, B.J.; Vienna, J.D. Binary phase diagram of the manganese oxide-iron oxide system. *J. Am. Ceram. Soc.* **2009**, *92*, 2378–2384, doi:10.1111/j.1551-2916.2009.03230.x.
23. Kjellqvist, L.; Selleby, M. Thermodynamic Assessment of the Fe-Mn-O system. *J. Ph. Equilib. Diffus.* **2010**, *31*, 113–134, doi:10.1007/s11669-009-9643-6.
24. Kang, Y.B.; Jung, I.H. Thermodynamic modeling of oxide phases in the Fe–Mn–O system. *J. Phys. Chem. Solids* **2016**, *98*, 237–246, doi:10.1016/j.jpcs.2016.07.017.
25. Wokon, M.; Kohzer, A.; Linder, M. Investigations on thermochemical energy storage based on technical grade manganese-iron oxide in a lab-scale packed bed reactor. *Sol. Energy* **2017**, *153*, 200–214, doi:10.1016/j.solener.2017.05.034.
26. Preisner, N.C.; Block, T.; Linder, M.; Leion, H. Stabilizing particles of manganese-iron oxide with additives for thermochemical energy storage. *Energy Technol.* **2018**, *6*, 2154–2165, doi:10.1002/ente.201800211.
27. Alonso, E.; Pérez-Rábago, C.; Licurgo, J.; Fuentealba, E.; Estrada, C.A. First experimental studies of solar redox reactions of copper oxides for thermochemical energy storage. *Sol. Energy* **2015**, *115*, 297–305, doi:10.1016/j.solener.2015.03.005.
28. Neises, M.; Tescari, S.; de Oliveira, L.; Roeb, M.; Sattler, C.; Wong, B. Solar-heated rotary kiln for thermochemical energy storage. *Sol. Energy* **2012**, *86*, 3040–3048, doi:10.1016/j.solener.2012.07.012.
29. Tescari, S.; Sundarraaj, P.; Moumin, G.; Duarte, J.P.R.; Agrafiotis, C.; de Oliveira, L.; Willsch, C.; Roeb, M.; Sattler, C. Solar rotary kiln for continuous treatment of particle material: Chemical experiments from

- micro to milli meter particle size. In Proceedings of the SOLARPACES 2019: International Conference on Concentrating Solar Power and Chemical Energy Systems, Daegu, Korea, 1–4 October 2019.
30. Jackson, G.S.; Imponenti, L.; Albrecht, K.J.; Miller, D.C.; Braun, R.J. Inert and reactive oxide particles for high-temperature thermal energy capture and storage for concentrating solar power. *J. Sol. Energy Eng.* **2019**, *141*, doi:10.1115/1.4042128.
 31. Alonso, E.; Gómez, F.; Gonzalez-Aguilar, J.; Romero, M. Experimental analysis of Mn_3O_4/MnO reduction in a packed-bed type solar reactor: Oxygen partial pressure influence. In Proceedings of the 2011 SolarPACES Conference, Granada, Spain, 20–23 September 2011.
 32. Oles, A.S.; Jackson, G.S. Modeling of a concentrated-solar, falling-particle receiver for ceria reduction. *Solar Energy* **2015**, *122*, 126–147, doi:10.1016/j.solener.2015.08.009.
 33. Schrader, A.J.; Dominicus, G.D.; Schieber, G.L.; Loutzenhiser, P.G. Solar electricity via an Air Brayton cycle with an integrated two-step thermochemical cycle for heat storage based on Co_3O_4/CoO redox reactions III: Solar thermochemical reactor design and modeling. *Sol. Energy* **2017**, *150*, 584–595, doi:10.1016/j.solener.2017.05.003.
 34. Nie, F.; Cui, Z.; Bai, F.; Wang, Z. Properties of solid particles as heat transfer fluid in a gravity driven moving bed solar receiver. *Sol. Energy Mater. Solar Cells* **2019**, *200*, 110007, doi:10.1016/j.solmat.2019.110007.
 35. Álvarez de Miguel, S. Analysis of redox reactions in a fluidized/fixed bed reactor for thermochemical energy storage in solar thermal power plants. Ph.D. Thesis, Universidad Politécnica de Madrid, Madrid, Spain, 2017.
 36. Cui, Z.; Shao, W.; Chen, Z.; Cheng, L. Mathematical model and numerical solutions for the coupled gas–solid heat transfer process in moving packed beds. *Appl. Energy* **2017**, *206*, 1297–1308, doi:10.1016/j.apenergy.2017.10.011.
 37. Negri, E.D.; Alfano, O.M.; Chiovetta, M.G. Moving-bed reactor model for the direct reduction of hematite. parametric study. *Ind. Eng. Chem. Res* **1995**, *34*, 4266–4276, doi:10.1021/ie00039a017.
 38. Takenaka, Y.; Kimura, Y.; Narita, K.; Kaneko, D. Mathematical model of direct reduction shaft furnace and its application to actual operations of a model plant. *Comput. Chem. Eng.* **1986**, *10*, 67–75, doi:10.1016/0098-1354(86)85047-5.
 39. Tong, A.; Sridhar, D.; Sun, Z.; Kim, H.R.; Zeng, L.; Wang, F.; Wang, D.; Kathe, M.V.; Luo, S.; Sun, Y.; et al. Continuous high purity hydrogen generation from a syngas chemical looping 25 kW_{th} sub-pilot unit with 100% carbon capture. *Fuel* **2013**, *103*, 495–505, doi:10.1016/j.fuel.2012.06.088.
 40. Zeng, L.; Tong, A.; Kathe, M.; Bayham, S.; Fan, L.S. Iron oxide looping for natural gas conversion in a countercurrent moving bed reactor. *Appl. Energy* **2015**, *157*, 338–347, doi:10.1016/j.apenergy.2015.06.029.
 41. Chen, C.; Lee, H.H.; Chen, W.; Chang, Y.C.; Wang, E.; Shen, C.H.; Huang, K.E. Study of an iron-based oxygen carrier on the moving bed chemical looping system. *Energy Fuels* **2018**, *32*, 3660–3667, doi:10.1021/acs.energyfuels.7b03721.

